Available online at www.sciencedirect.com

ScienceDirect

Biochimica et Biophysica Acta 1757 (2006) 1035–1046

BIOCHIMICA ET BIOPHYSICA ACTA

BBA

www.elsevier.com/locate/bbabio

Review

Combined DFT and electrostatics study of the proton pumping mechanism in cytochrome *c* oxidase

Jason Quenneville [1], Dragan M. Popović, Alexei A. Stuchebrukhov *

Department of Chemistry, University of California, One Shields Avenue, Davis, CA 95616, USA

Received 4 October 2005; received in revised form 5 December 2005; accepted 14 December 2005
Available online 18 January 2006

Abstract

Cytochrome *c* oxidase is a redox-driven proton pump which converts atmospheric oxygen to water and couples the oxygen reduction reaction to the creation of a membrane proton gradient. The structure of the enzyme has been solved; however, the mechanism of proton pumping is still poorly understood. Recent calculations from this group indicate that one of the histidine ligands of enzyme's Cu_B center, His291, may play the role of the pumping element. In this paper, we report on the results of calculations that combined first principles DFT and continuum electrostatics to evaluate the energetics of the key energy generating step of the model—the transfer of the chemical proton to the binuclear center of the enzyme, where the hydroxyl group is converted to water, and the concerted expulsion of the proton from δ-nitrogen of His291 ligand of Cu_B center. We show that the energy generated in this step is sufficient to push a proton against an electrochemical membrane gradient of about 200 mV. We have also re-calculated the pK_a of His291 for an extended model in which the whole Fe_{a3}–Cu_B center with their ligands is treated by DFT. Two different DFT functionals (B3LYP and PBE0), and various dielectric models of the protein have been used in an attempt to estimate potential errors of the calculations. Although current methods of calculations do not allow unambiguous predictions of energetics in proteins within few pK_a units, as required in this case, the present calculation provides further support for the proposed His291 model of *CcO* pump and makes a specific prediction that could be targeted in the experimental test.

Keywords: Cytochrome *c* oxidase; DFT/electrostatic calculation; Proton pumping; Redox-coupled pK_a; pK_a calculation

1. Introduction

Cytochrome *c* oxidase (*CcO*) is the terminal enzyme of the respiratory electron transport chain of aerobic organisms; it catalyses the reduction of oxygen to water, and couples this reaction to proton pumping across the membrane, a process which results in the membrane proton gradient [1–5]. In the course of its catalytic activity, electrons delivered by cytochrome *c* are transferred via Cu_A and heme *a* to the heme a_3-Cu_B catalytic site, where the reduction of oxygen takes place, see Fig. 1. In the catalytic cycle, the transfer of each of the four electrons required for the reduction of oxygen is accompanied by the translocation of two protons, of which one is consumed internally in the Fe_{a3}–Cu_B center for the reduction of oxygen and the other is pumped across the membrane [4,5]. The overall reaction can be expressed as follows:

$$O_2 + 4e^- + 8H^+(\text{in}) \rightarrow 2H_2O + 4H^+(\text{out}) \quad (1)$$

where (in) and (out) indicate two sides of the membrane, the matrix and periplasmic side, respectively. Both chemical and pumped protons are delivered along the *K*- and *D*-channels, of which the majority (up to 7 protons) are moving along the *D*-channel [6,7].

In the past decade, the structure of *CcO* has been solved for several organisms, however, the molecular mechanism of proton pumping remains a subject of intense debate. A detailed review

Abbreviations: *CcO*, cytochrome *c* oxidase; DFT, density functional theory; MeIm, methylimidazole; QM, quantum mechanical; PBE, Poisson–Boltzmann equation; PRD, heme propionate D; SCRF, self-consistent reaction field; The numbering refers to bovine *CcO*

* Corresponding author. Fax: +1 530 752 8995.
E-mail address: stuchebr@chem.ucdavis.edu (A.A. Stuchebrukhov).
[1] Present address: Applied Physics Division, Los Alamos National Laboratory, Los Alamos, NM 87545, USA.

0005-2728/$ - see front matter © 2005 Elsevier B.V. All rights reserved.
doi:10.1016/j.bbabio.2005.12.003

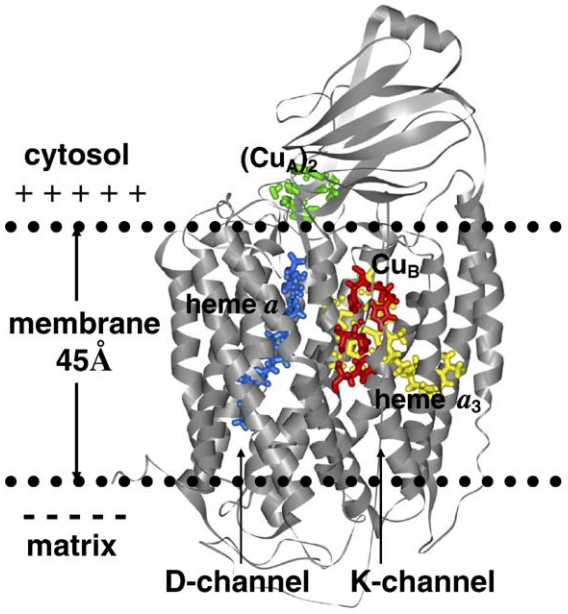

Fig. 1. Chains A and B of bovine heart cytochrome *c* oxidase [30] in the mitochondrial membrane. The four redox centers from left to right: Cu_A complex (green), heme *a* (blue), heme a_3 (yellow), Cu_B complex (red), form the electron transport pathway. In the present study, the latter two are treated with density functional theory. The rest of the protein is represented by partial atomic charges embedded in the inhomogeneous dielectric of the protein–membrane–solvent system and treated by electrostatic calculation.

of the enzyme structure together with recent experimental work on the kinetics of coupled electron and proton transfer reactions in the enzyme can be found in the literature [1–3,6–10].

In a recent work from this group [11–13], on the basis of electrostatic and ab initio calculations, a kinetic model of proton pumping by *CcO* was proposed. The key elements of the model, see Fig. 2A, are the calculated redox dependent changes of the protonation state of His291 (bovine notation), a Cu_B ligand, and the predicted two chains of water molecules [14,15] connecting Glu242 both to the catalytic site and to His291 (via PRD of heme a_3 and Arg438 groups). Glu242 is an experimentally established proton donor, both for pumping and for chemistry [16–19]. The structure of proton conducting paths suggests that the rate of proton transfer from Glu242 to His291 is likely much faster than that between Glu242 and the hydroxyl group in the catalytic center. The following model therefore was proposed: upon electron transfer between heme *a* and the catalytic center, *two* proton transfers occur sequentially: first, a proton is transferred between Glu242 and His291, then, after re-protonation of Glu242, a second proton is transferred to the binuclear catalytic site, where water is formed. The Coulomb repulsion between the proton residing on His291 and the proton in the catalytic center results in the "expulsion" of the former in the direction of the positive side of the membrane, and eventually giving rise to a pumping event. The energetic feasibility of such proton transfer events has gain further support in a combined DFT/electrostatic calculations of redox dependent pK_a values of Glu242 and His291 [13]. The proton exit path from His291 to the positive side of the membrane and a possible mechanism of preventing the "leaking" of protons from the positive side of the membrane to the negative side through the proton conducting channels of the enzyme were discussed in Ref. [20]. The catalytic cycle based on this model is discussed in Ref. [12]. One transition of the cycle, F to H, which includes a single proton pumping event discussed in the present paper, is shown in Fig. 2B.

In this paper, we report on the results of calculations that combined first principles DFT and continuum electrostatics to evaluate the energetics of the key energy generating step of the model—the transfer of the chemical proton to the binuclear center of the enzyme, where the hydroxyl group is converted to water, and the concerted expulsion of the proton from δ-nitrogen of His291 ligand of Cu_B center. We show that the energy generated in this step is sufficient to push a proton against an electrochemical membrane gradient of about 200 mV. We have also re-calculated the pK_a of His291 for an extended model in which the whole Fe_{a3}–Cu_B center with their ligands is treated by DFT. Two different DFT functionals (B3LYP and PBE0), and various dielectric models of the protein have been used in an attempt to estimate potential errors of the

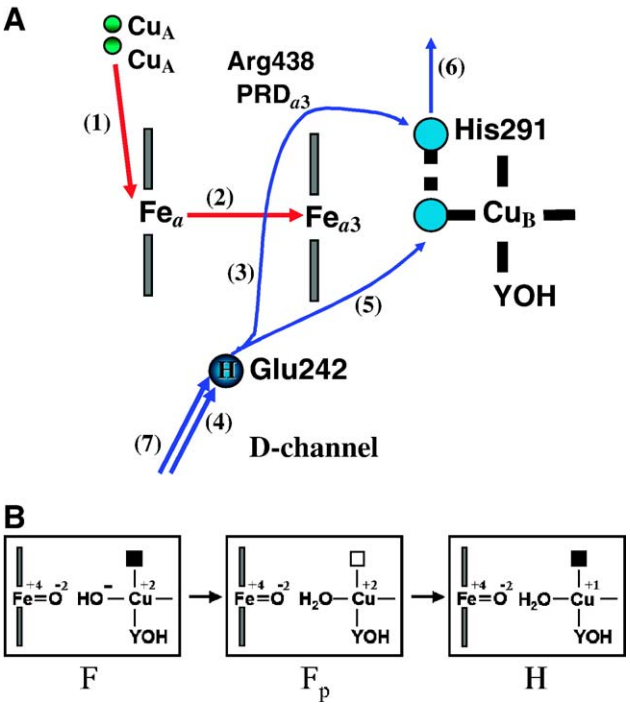

Fig. 2. (A) The schematics of the proposed proton-pumping mechanism of *CcO*. The sequence of transitions during one pumping cycle of the enzyme is shown. Upon the ET to binuclear center (red arrows), two protons are translocated nearby the active site (blue arrows). Presumably, the Glu242 is a proton donor in this process, while two protonatable sites are His291 (proton-loading site) and OH^- ligand of the binuclear center. The key assumption of the model is that the PT rate of the pumping proton is much higher than the rate of the chemical proton ($k_3 \gg k_5$). (B) Schematic of the states of the catalytic cycle that are studied in this paper. The heme a_3 Fe–porphyrin is shown at the left, the Cu_B complex on the right. The proposed proton-loading site, His291, is depicted with either a filled square (protonated) or an empty square (deprotonated). For complete catalytic cycle, see Ref. [12]. The *F* state is shown in Table 6. The OORO and OORR redox states (in our notation) which appear in Tables 2–5, refer fo F_p and H state, respectively. Tables 7 and 8 display the reaction free energy (ΔG_R) of the proton pumping step, i.e., $F \rightarrow F_p$ transition.

calculations. Although current methods of calculations do not allow unambiguous predictions of energetics in proteins within few pK_a units, as required in this case, the present calculation does support the proposed His291 model of *CcO* pump.

The structure of the paper is as follows: in the next section, we describe the DFT/electrostatic method and the computational models that were used in our work, while in Results and Discussion Section we present and discuss the obtained results from our studies on *CcO*. A summary of the results, together with concluding remarks, is given in the last section.

2. Methods and models

The combination of DFT and electrostatic calculations has been used successfully in the past to compute the pK_a values and redox potentials in various enzymes and proteins [21–25]. This approach takes advantages of both methods by combining the accuracy of quantum chemical calculations with a detailed description of electrostatic interactions of the whole protein. Density functional theory is applied to a relatively small quantum-mechanical system (QM) of interest to optimize its geometry, to evaluate electronic energies, and to obtain the atomic partial charges for different redox and protonation states of the complex. Electrostatic calculations, on the other hand, are used to evaluate the solvation energy of the complex in the protein environment and the Coulomb interactions of the QM complex with protein charges. Both the polarization of the protein medium and the protein charges affect the electron distribution of the complex, therefore the electrostatic and DFT calculations are carried in a self-consistent way. This method was shown to produce pK_a values in proteins that are generally in good agreement with experimental data [22,25–28].

2.1. Overview

Here, we briefly summarize the DFT/electrostatic method of pK_a calculations, mainly to introduce notation for different energy terms, which are discussed later in the text. A more detailed discussion can be found in our recent publication on this subject [13].

In the calculation we divide the whole system into an active site complex (QM system) and the surrounding medium—protein, membrane, and the external aqueous phase. The proton affinity of the complex is calculated with an accurate DFT method, and the dielectric effects of medium are treated with classical electrostatic methods. The protein medium includes partial atomic charges, charges of redox centers, and charges of the titratable groups, which directly affect the electronic energies of the complex.

The dielectric medium involves protein itself, the membrane, and the surrounding solvent. The protein by itself is an inhomogeneous dielectric because it has many internal cavities, which contain water molecules. These regions should have higher dielectric constant than the regions of "dry" protein. For regions of dry protein, a specific value of dielectric constant ε_{prot} is assumed, and for the cavities a higher value ε_{cavity} is used. Neither of these values is well defined, although ε_{prot} should be close to 4, while the cavities can have dielectric constant ε_{cavity} anywhere from 4 to 80. The upper value would correspond to dielectric response equivalent to that of the bulk water.

The pK_a value is related to the free energy of deprotonation, which is a sum of two contributions: the free energy of deprotonation in vacuum (ΔG^{deprot}_{vac}), and the solvation energy difference between the deprotonated and protonated forms of the protonatable group ($\Delta\Delta G^{deprot}_{solv}$), see also [25,29]:

$$pK_a = \frac{1}{kT\ln 10}\left(\Delta G^{deprot}\right) = \frac{1}{kT\ln 10}\left(\Delta G^{deprot}_{vac} + \Delta\Delta G^{deprot}_{solv}\right) \quad (2)$$

The pK_a value of the group of interest can be calculated by comparing the above terms for a suitable model compound, for which the pK_a value is experimentally known, and the corresponding values of the group of interest. In fact, the *shift* of pK_a value is calculated:

$$pK_a^{site} = pK_a^{model} + \Delta pK_a. \quad (3)$$

The relative shift of the group's pK_a with respect to the model compound can be expressed as

$$\Delta pK_a = \frac{1}{kT\ln 10}\Delta\Delta G_{shift} = \frac{1}{kT\ln 10}\left(\Delta\Delta E_{elec} + \Delta\Delta G_{solv}\right), \quad (4)$$

where $\Delta E_{elec} = \Delta E^{A^-}_{elec} - \Delta E^{HA}_{elec}$ is a quantum-mechanically (QM) calculated electronic energy difference in the gas phase between the deprotonated and protonated forms, and $\Delta\Delta E_{elec}$ is its shift relative to the model compound; $\Delta G_{solv} = \Delta G^{A^-}_{solv} - \Delta G^{HA}_{solv}$ is the difference in solvation energy between the deprotonated and protonated forms, and $\Delta\Delta G_{solv}$ is the shift of the solvation energy relative to the model compound. (In the above Eq., when the *difference* of pK_as is computed between two compounds, the free energy of a solvated proton as well as some entropy contributions cancel out; thus, e.g., only electronic energy, i.e., the enthalpic part, of the vacuum term remains. If the two compounds have a different chemical structure (functional group), one should also add the difference due to vibrational contribution—usually, the difference in zero-point energy. Typically this term is rather small, see below.)

The total solvation energy (x=deprotonated or protonated form) is divided into several components:

$$G^x_{solv} = G^x_{Born} + G^x_{strain} + G^x_q. \quad (5)$$

The Born solvation energy (G^x_{Born}), and the energy of interaction with protein charges (G^x_q) are two main contributions to the free energy of solvation of the active site complex in the protein environment. The third term (G^x_{strain}) is the so-called strain energy; this term reflects the energy associated with the reorganization of electron density of the QM system induced by the reaction field of the polarized medium. (The origin of this term is as follows. The charges of the QM system polarize the surrounding medium, in turn, the induced polarization of the medium slightly changes the charge distribution of the QM system, compared with the initial charge distribution in vacuum.)

The pK_a of the active site complex can then be calculated as,

$$pK_a^{site} = pK_a^{model} + \frac{1}{kT\ln 10}\left(\Delta\Delta E_{elec} + \Delta\Delta G_{strain} + \Delta\Delta G_{Born} + \Delta\Delta G_q\right) \quad (6)$$

where first two energy terms are evaluated by using quantum chemistry and last two terms are obtained from solvation electrostatic calculations. Alternatively, one can calculate the absolute value of pK_a [29]. We have confirmed that both methods – the absolute and relative pK_a's – give practically identical results. In the calculations using Eq. (6), the protonation state of the protein residues other than the site of interest, are pre-calculated using a standard self-consistent continuum electrostatics method as described in Ref. [11]. In the following we will be using the above expression and the relative method. For calculation of pK_a of His291, the model compound 4-methylimidazole will be used, Scheme 1.

2.2. Density functional calculations

The starting structure of the active site was taken from the X-ray crystal structure of bovine heart cytochrome *c* oxidase obtained by Yoshikawa, et al, at 2.3 Å resolution (PDB code, 2OCC) [30]. The QM-model (Fig. 3) used to calculate the pK_a of a Cu_B ligand consists of the Cu atom, methylimidazole

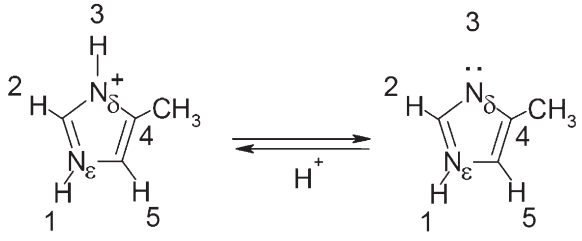

Scheme 1. Deprotonation of the 4-methylimidazole molecule.

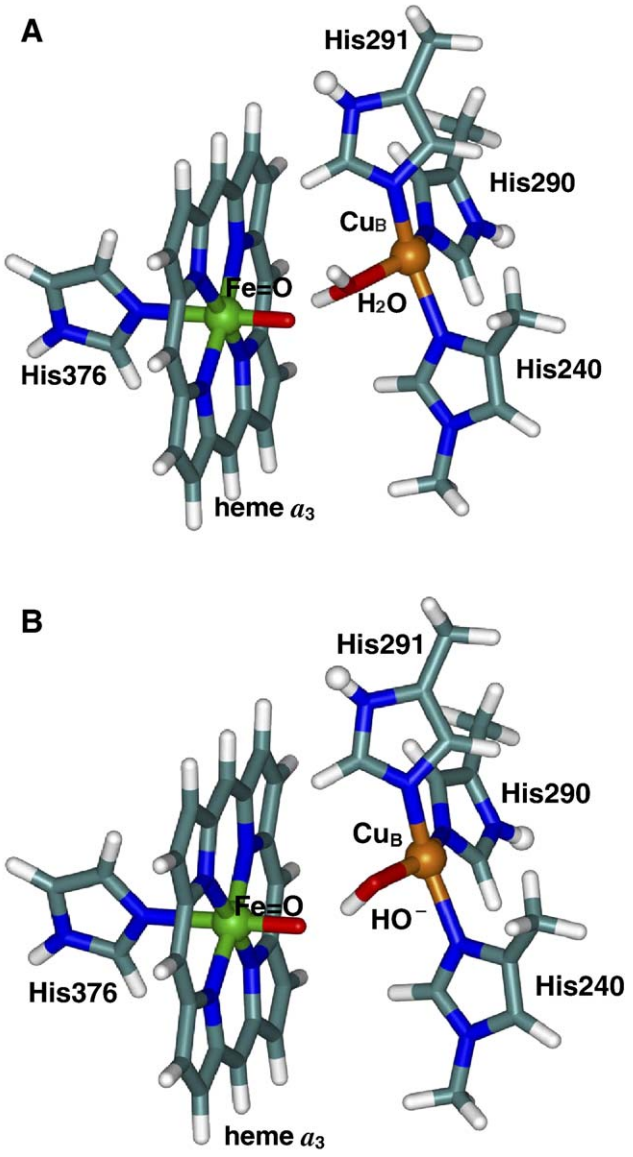

Fig. 3. (A) Binuclear center of *CcO*, with iron(IV)-oxo heme a_3 and H_2O Cu_B ligand. This geometry was used to calculate the energy for the F_P and H states. The two metal atoms, Fe_{a3} and Cu_B, are shown as large spheres; the protonatable site of His291 is shown with smaller sphere. (B) Binuclear center of *CcO*, with iron(IV)-oxo heme a_3 and OH^- Cu_B ligand. This geometry was used to calculate the energy for the F state.

molecules representing coordinated histidines 240, 290 and 291, a methyl group representing tyrosine 244 (which is cross-linked to His240), and an H_2O or OH^- Cu_B-ligand. The methyl groups attached to the imidazoles represent the β-methylene groups of histidine. Compared with our previous calculations [13], the new larger quantum-chemical system also includes ferryloxy porphyrin part and an imidazole ring that represents His376 (the sixth ligand to Fe_{a3} metal ion).

In the present calculations, tyrosine 244 is replaced by methyl-group only in the QM system, but it is present in electrostatic solvation calculations. Is it legitimate to make this replacement? First of all, we consider only the states of the catalytic cycle where Tyr244 is neutral (protonated), and not in $TyrO^\bullet$ or $TyrO^-$ state (thus, P_m and P_r states are not considered). Second, Tyr is not directly bound to Cu_B atom, but it is cross-linked to the His240 ligand of Cu_B, and it is quite distant from His291 site on which the protonation changes occur. Therefore, it is reasonable to assume that the electronic density on Tyr244 will not significantly change between the two states of the protonated and deprotonated His291 site.

Energies of each coupled protonation/redox state of the complex were calculated using density functional theory (DFT) [31,32] and the Jaguar 5.5 quantum chemistry package [33]. Both the B3LYP [34] and PBE0 [35] hybrid density functionals were employed, and all calculations used unrestricted wavefunctions. While the B3LYP functional has been used almost exclusively for this system in the past [13,29,36–38], the use of the PBE0 functional has grown significantly in recent years. Unlike B3LYP, the PBE0 functional has the attractive quality of having only one parameter with respect to the exchange-correlation. Furthermore, despite the success of B3LYP, for many quantities (including proton affinities), the PBE0 functional can give comparable or superior results [39,40]. For the Fe and Cu metal atoms, the LACV3P+* basis set, which includes non-relativistic electron core potentials, was used for reported single point energies [33,41]. For the remaining atoms, the 6–311+G* (see Jaguar [33] or Refs. [42–45]) basis set was used. Thus all non-hydrogen atoms had both diffuse and polarization functions.

Geometry optimizations were carried out in the Cartesian space in vacuum, and therefore without the surrounding charges of the protein. All optimizations used the 6–31+G* (see Jaguar [33] or Refs. [46–51]) (for non-metal atoms) and LACVP+* (for Fe and Cu) basis sets in both the B3LYP and PBE0 calculations.

First, the geometry of the porphyrin of heme a_3, along with the iron-ligated His376 residue, was optimized for the $[Fe{=}O]^{+2}$ (iron(IV)-oxo) state of iron, but without the Cu_B complex present. Separate optimizations were conducted for the singlet, triplet and quintet spin states to verify that our DFT method predicted the ordering of the spin states correctly. Our findings compared well to literature values, Refs. [52,53], and therefore all calculations presented in this paper use the triplet state of the iron(IV)-oxo porphyrin.

After the initial optimization of the Fe_{a3}–porphyrin group, the whole Fe_{a3}–Cu_B complex, together with the ligands, were re-optimized. During the optimization, to preserve the overall experimental structure of the complex, some atoms were fixed at their positions as reported in the crystal structure. The frozen atoms include the two methyl groups of the methylimidazoles (for His290 and His291), as well as the entire dimethylimidazole ligand (representing His240 and Tyr244). In addition, the two ε-nitrogens, which ligate His290 and His291 to Cu_B, are also kept fixed to avoid tetrahedral-like geometries of the Cu center. In addition, the Fe–porphyrin/His376 moiety was included in the geometry optimizations, with all the atoms fixed except for the Fe=O group.

The side chain of the Val243 residue (modeled here by a propane molecule) was included explicitly in the DFT geometry optimizations, to ensure proper arrangement and avoid a possible van der Waals clashes of OH^-/H_2O ligand of Cu_B center (see Fig. 4). Attempts at optimizing the H_2O ligand without Val243 present often led to dissociation of the Cu–OH_2 bond and incorrect orientation of water molecule (i.e., with van der Waals overlaps) in the catalytic site.

Hydrogen bonding between the OH^-/H_2O ligand of oxidized Cu_B and the ferryloxy oxygen is strong, with interoxygen distances of 2.6 Å for H_2O and 2.7 Å for OH^- species. Finally, for the optimizations pertaining to the reduced state of Cu_B, the O atom of the H_2O ligand was fixed to the coordinates obtained when Cu_B was oxidized. This was done because the reduced state of Cu_B does not bind H_2O tightly, and we wanted to ensure comparable geometries between the two redox states. We believe that without this constraint and by not including all residues surrounding the catalytic center, the H_2O molecule would have more freedom in our optimizations than it otherwise should.

To quantify the effect of the electronic reorganization of the QM system, and to obtain the corresponding set of the ESP fitted charges, the complex was surrounded by a continuum dielectric and the self-consistent reaction field (SCRF) method was applied as implemented in Jaguar 5.5 [54,55]. (Unfortunately, this program does not allow treatment of inhomogeneous dielectrics. We have now modified the program and find that the self-consistent QM charges calculated in an inhomogeneous dielectric of the protein, and in the presence of other charges of the protein, do not change qualitative conclusions of this paper. Quantitatively, the results change only insignificantly.) The probe radius of the surrounding dielectric was set to 1.4 Å, and the standard Jaguar set of the van der Waals radii for atoms was used. The ESP atomic charges were generated by using a modified version of the CHELPG procedure of Breneman and Wiberg [56].

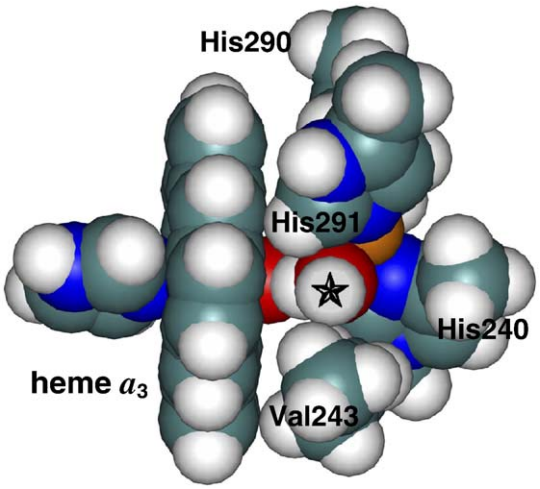

Fig. 4. Space-filled rendering of the binuclear center using van der Waals radii. The figure shows how the Val243 residue affects the orientation of the H_2O Cu_B ligand. The proton that converts the OH^- ligand to H_2O is marked with a star. Without inclusion of the Val243 side chain (shown here as a propane molecule), we were not able to obtain an appropriate geometry of the H_2O/OH^- ligand.

The final computations were performed on five different structures: [Fe═O $(H_2O)Cu^{2+}$ (HisH)], [Fe═O $(H_2O)Cu^{2+}$ (His^-)], [Fe═O $(H_2O)Cu^+$ (HisH)], [(Fe═O $(H_2O)Cu^+$ (His^-)] and [Fe═O $(HO^-)Cu^{2+}$ (HisH)], which represent different oxidation states of Cu_B center, different protonation states of His291 site, and H_2O/OH^- ligand of Cu_B.

2.3. Continuum electrostatic calculations

The electrostatic calculations have been performed by using program MEAD [57,58], as described in Ref. [13]. To correctly describe the effects of the protein charges on the pK_a's of selected groups, the protonation state of all *other* titratable groups of the enzyme, for a given redox state of metal centers, is required. To this end, we performed the standard continuum electrostatic calculations as described in Ref. [11]. In different redox states, the equilibrium proton distribution is slightly different due to the proton uptake from the solution (aqueous phase), and much different from the standard protonation state.

The electrostatic calculations were performed on chains *A* and *B* of bovine heart *CcO* (PDB code, 2OCC) [30]. The two chains were embedded into a membrane, and solvated in water. In our calculations, the membrane is modeled as a low dielectric slab of 45 Å that covers the central part of the enzyme, Fig. 1.

Once the charges of the QM system have been calculated, its geometry optimized, and the equilibrium charge distribution of the protein has been determined, the solvation energy of the QM system in the protein can be calculated. For solvation, the MEAD program [58] has been used. The solvation energy in the protein consists of two main contributions—the Born solvation energy, and the energy of interaction with the protein charges.

To find these contributions, the Poisson equation (or PBE) is solved numerically. The dielectric constants of 1, 4 and 80, were used for the QM system, the protein-membrane, and the solvent region, respectively [59–62]. In addition to these typical values for the dielectric regions, we also examined the dependence of the results on the various values of the dielectric constant associate with water filled cavities inside of the protein.

In these calculations, the ESP fitted charges are used for the QM-system, while partial charges of the protein atoms are taken from the CHARMM22 parameter set [63], modified so as to reflect the equilibrium protonation state of the enzyme [11]. The protein charges [64] and radii [63] that we use in this application have been used successfully before to calculate the electrostatic energies, protonation probabilities of titratable groups and redox potentials of cofactors in different proteins [11,64–67]. For all other details of the electrostatic calculations, the reader is referred to our recent publication, Ref. [13].

3. Results and discussion

In order to analyze the effect of different factors on the pK_a values, we considered several computational models, as we did in Ref. [13]. Thus, the reported here pK_a values of His291 residue and OH^- group were calculated in: (1) a continuum aqueous solution; (2) a continuum low dielectric of $\varepsilon=4$ without protein charges; (3) an inhomogeneous dielectric of protein, $\varepsilon=4$ and 80 but without protein charges; (4) a continuum $\varepsilon=4$ including protein charges; (5) and in the "real" protein including dielectric inhomogeneities and protein charges (see Fig. 3 in Ref. [13] for the different solvation models). In addition, we have probed different dielectric models of the water cavities in the enzyme by varying the corresponding dielectric constant in the range of 10 to 80. Data are presented for DFT-B3LYP and DFT-PBE0 functionals.

3.1. The calculation of pK_a in water

For the sake of completeness, and for convenience of comparison with other workers, we first report the pK_a values of the Cu_B histidine ligand in oxidized (Fe═O $(H_2O)Cu^{2+}$ (HisH)) and reduced (Fe═O $(H_2O)Cu^+$ (HisH)) binuclear complex in the aqueous phase. For calculations of the pK_a values of δ-nitrogen of His291 ligand of Cu_B center, we use MeIm as a reference compound, for which the experimental pK_a is known. The experimental pK_a value of δ-nitrogen of MeIm is 6.6 [68]. Using this value and the difference in electronic and solvation energies between MeIm and Fe_{a3}–Cu_B model complex, as explained in Methods and models, one can evaluate the pK_a value of the latter in the aqueous phase. The results for both, B3LYP and PBE0, density functionals are presented in Table 1. The protonated and deprotonated forms of MeIm refer to cationic and neutral (δ-nitrogen deprotonated) forms of MeIm, see Scheme 1, while the two protonation forms of binuclear model complex refer to protonated and deprotonated δ-nitrogen of His291 ligand.

The side chain of an isolated histidine in water has two macroscopic pK_a values of 7.0 and 14.0, for the first and the second deprotonation [69]. For isolated methylimidazole, the pK_a in water has been measured to be 6.6 (for the Nδ-site proton) [68]. We find that methylimidazole model of His291 ligand of the binuclear Fe_{a3}–Cu_B complex possesses pK_as of 8.89 (from B3LYP calculations) or 8.0 (from PBE0 calculations) in oxidized Fe═O $(H_2O)Cu^{2+}$ (HisH) form and 14.38 (B3LYP) or 15.95 (PBE0) in reduced Fe═O $(H_2O)Cu^+$ (HisH) form, based on our present DFT/electrostatic calculations. The obtained results for the extended model of Fe_{a3}–Cu_B binuclear complex considered here are in good agreement with the results of our previous calculations performed on the smaller Cu_B complex [13,29].

3.2. The pK_a of His291 in CcO

Tables 2 and 3 summarize the results of the electrostatic solvation calculations, using ESP charges from both B3LYP and PBE0 density functionals, and for two different dielectric

Table 1
The obtained solvation and electronic energy terms of 4-methylimidazole and Fe_{a3}–Cu_B complex in oxidized or reduced form used in the DFT/electrostatic calculations (see Eq. (6)) to evaluate the aqueous phase pK_a values of Histidine site in the Fe_{a3}–Cu_B complex relative to the experimental pK_a of the model compound (MeIm)

Compound	$E_{reorg.}$		ΔG_{strain}	ΔG_{Born}	ΔG_{solv}	$\Delta\Delta G_{solv}$	ΔE_{elec}	$\Delta\Delta E_{elec}$	$\Delta\Delta G_{shift}$	ΔpK_a	pK_a
	Depr.	Prot.									
B3LYP											
4-methylimidazole	+4.00	+1.50	+2.50	+52.33	+54.83	0	+234.60	0	0	0	6.6 [a]
Fe═O $Cu_B^{2+}(H_2O)$ complex	+7.13	+5.13	+2.00	+70.18	+72.18	+17.35	+220.40	−14.20	+3.15	+2.29	8.89 [b]
Fe═O $Cu_B^{+}(H_2O)$ complex	+10.40	+5.71	+4.69	+4.72	+9.41	−45.42	+290.70	+56.10	+10.68	+7.78	14.38 [b]
PBE0											
4-methylimidazole	+3.49	+1.30	+2.19	+51.30	+53.49	0	+231.37	0	0	0	6.6 [a]
Fe═O $Cu_B^{2+}(H_2O)$ complex	+7.46	+2.77	+4.69	+65.98	+70.67	+17.18	+216.11	−15.26	+1.92	+1.40	8.00 [b]
Fe═O $Cu_B^{+}(H_2O)$ complex	+10.66	+6.16	+4.50	+2.46	+6.96	−46.53	+290.74	+59.37	+12.84	+9.35	15.95 [b]

Data are shown for the DFT-B3LYP and PBE0 density functionals. Energies are reported in kcal/mol.
[a] Experimental value.
[b] Calculated value.

models of the protein. Namely, the solvation energies of the Fe_{a3}–Cu_B complex are calculated and compared for a uniform low dielectric medium of ε=4, and for the "real" protein model. Both models include the surrounding protein charges; however, only the latter model includes the inhomogeneity of the dielectric environment of the protein–membrane–solvent system. It is interesting to examine the differences between the two models.

The qualitative features of the solvation models discussed previously for a smaller Cu_B complex [13], are still valid for a larger QM Fe_{a3}–Cu_B complex considered here. The Born solvation energy is generally larger in the inhomogeneous dielectric model of the protein than in the uniform ε=4 model. The related result is that the energy of interaction with protein charges in the inhomogeneous model is much smaller than that in the uniform ε=4 model, obviously due to the screening effect of water-filled cavities. For more detail discussion, see Refs. [13,29].

In Table 4 (B3LYP) and Table 5 (PBE0), the effects of different dielectric and protein charge models on the pK_a of His291, which is a part of Fe_{a3}–Cu_B complex, are shown. The tables list all energy terms needed to compute the relative pK_as of the complex with respect to the MeIm model compound.

In B3LYP, the calculated pK_a values of His291 ligand of the Fe_{a3}–Cu_B complex in *CcO* are found to be 5.4 and 21.9 for oxidized (Fe═O $(H_2O)Cu^{2+}$ (HisH)) and reduced (Fe═O $(H_2O)Cu^{+}$ (HisH)) complexes, respectively. In PBE0, the corresponding values are 5.0 and 26.1. These values compare reasonably well with 2.1 (for the OORO redox state of the protein) and 17.4 (OORR) obtained previously for the Cu_B center alone [13]. Thus, we confirm that the protonation state of His291 is redox dependent, when the full protein model, with charges, and dielectric inhomogeneities is used.

Table 2
The solvation (kcal/mol) of the Fe_{a3}–Cu_B complex in low dielectric continuum of ε=4 and in the protein including the protein charges

Compound	G_{Born}	G_q	G_{strain}	G_{solv}
OORO redox state [a]				
Fe═O $Cu_B^{2+}(H_2O)$(His291$^-$)	−42.81 [b]	−33.69	+3.25	−73.25
	−49.04 [b]	**−14.49**	**+3.25**	**−60.28**
Fe═O $Cu_B^{2+}(H_2O)$(His291H)	−98.18	−64.00	+2.50	−159.68
	−109.43	**−20.75**	**+2.50**	**−127.68**
Δ(Depr.-Prot.) oxidized	+55.37	+30.31	+0.75	+86.43
	+60.39	**+6.26**	**+0.75**	**+67.40**
OORR redox state [a]				
Fe═O $Cu_B^{+}(H_2O)$(His291$^-$)	−29.67	−6.99	+3.51	−33.15
	−33.42	**−9.01**	**+3.51**	**−38.92**
Fe═O $Cu_B^{+}(H_2O)$(His291H)	−39.11	−38.38	+2.64	−74.85
	−44.77	**−16.54**	**+2.64**	**−58.67**
Δ(Depr.-Prot.) reduced	+9.44	+31.39	+0.87	+41.70
	+11.35	**+7.53**	**+0.87**	**+19.75**

The total solvation consists of two main contributions: the Born solvation energy, and the interaction with protein charges (so-called reaction and protein field). The protein charges reflect the equilibrium protonation state of the enzyme for the OORO and OORR redox state of metal centers. Solvation energies are computed with DFT-B3LYP functional ESP fitted partial atomic charges of the Fe_{a3}–Cu_B complex.
[a] Redox states OORO and OORR refer to the state of four redox-active metal centers: Cu_A, heme *a*, heme a_3 and Cu_B complex, respectively.
[b] Results for the continuum dielectric of ε=4 are shown in normal font letters, while solvation energies for protein environment are shown in bold.

Table 3
Same as in Table 2, only for PBE0 functional

Compound	G_{Born}	G_q	G_{strain}	G_{solv}
OORO redox state				
Fe═O $Cu_B^{2+}(H_2O)$(His291$^-$)	−44.13	−33.72	+3.70	−74.15
	−50.52	**−14.58**	**+3.70**	**−61.40**
Fe═O $Cu_B^{2+}(H_2O)$(His291H)	−98.48	−64.03	+2.55	−159.96
	−109.69	**−20.81**	**+2.55**	**−127.95**
Δ(Depr.-Prot.) oxidized	+54.35	+30.31	+1.15	+85.81
	+59.17	**+6.23**	**+1.15**	**+66.55**
OORR redox state				
Fe═O $Cu_B^{+}(H_2O)$(His291$^-$)	−30.72	−6.48	+4.62	−32.58
	−34.63	**−8.51**	**+4.62**	**−38.52**
Fe═O $Cu_B^{+}(H_2O)$(His291H)	−39.91	−38.56	+2.89	−75.58
	−45.65	**−16.72**	**+2.89**	**−59.48**
Δ(Depr.-Prot.) reduced	+9.19	+32.08	+1.73	+43.00
	+11.02	**+8.21**	**+1.73**	**+20.96**

Table 4
The pK_a values of His291 residue of oxidized and reduced Fe_{a3}–Cu_B center in cytochrome *c* oxidase

Redox state	ΔE_{elec}	$\Delta\Delta E_{elec}$	ΔG_{solv}	$\Delta\Delta G_{solv}$	$\Delta\Delta G_{shift}$	ΔpK_a	pK_a
In aqueous phase							
4-methylimidazole	+234.6	0	+54.83	0	0	0	6.6
Fe=O $Cu_B^{2+}(H_2O)$ oxidized	+220.4	−14.2	+72.18	+17.35	+3.15	+2.29	8.89
Fe=O $Cu_B^{+}(H_2O)$ reduced	+290.7	+56.1	+9.41	−45.42	+10.68	+7.78	14.38
In continuum dielectric of ε=4 (no protein charges)							
Fe=O $Cu_B^{2+}(H_2O)$ oxidized	+220.4	−14.2	+56.12	+1.29	−12.91	−9.40	−2.80
Fe=O $Cu_B^{+}(H_2O)$ reduced	+290.7	+56.1	+10.31	−44.52	+11.58	+8.44	15.04
In inhomogeneous dielectric of protein, ε=4 and 80 (no protein charges)							
Fe=O $Cu_B^{2+}(H_2O)$ oxidized	+220.4	−14.2	+61.14	+6.31	−7.89	−5.75	0.85
Fe=O $Cu_B^{+}(H_2O)$ reduced	+290.7	+56.1	+12.22	−42.61	+13.49	+9.83	16.43
In continuum ε=4 (including protein charges)							
OORO	+220.4	−14.2	+86.43	+31.60	+17.40	+12.67	19.27
OORR	+290.7	+56.1	+41.70	−13.13	+42.97	+31.30	37.90
In protein (including dielectric inhomogeneity and protein charges)							
OORO	+220.4	−14.2	+67.40	+12.57	−1.63	−1.20	5.40
OORR	+290.7	+56.1	+19.75	−35.08	+21.02	+15.31	21.91
OORO (ε_{cavity}=20)	+220.4	−14.2	+71.35	+16.52	+2.32	+1.69	8.29
OORR (ε_{cavity}=20)	+290.7	+56.1	+24.45	−30.38	+25.72	+18.73	25.33

The pK_a of His291 is calculated relative to the pK_a of the model compound—methylimidazole in aqueous phase (see Eq. (6)). It is shown how different dielectric environments and interaction with protein charges affect the calculated pK_a of the His291 site. Energies are reported in kcal/mol for the B3LYP density functional calculations on the binuclear complex.

From different models presented in Tables 4 and 5, one can see that the pK_a of His291 is also redox-dependent in a continuum low dielectric without protein charges, as well as in the inhomogeous dielectric model without protein charges. The histidine ligand to Cu_B in Fe_{a3}–Cu_B complex solvated in aqueous phase is always protonated independently from its redox state. It is important to notice that the high pK_as of His291 in both redox states are also obtained in an over-simplified model when the protein is modeled as a continuum low dielectric medium with appropriate protein charges.

We also find that for our model to work, i.e., for His291 to have redox-dependent protonation state, one need to assume the dielectric constant of water cavities in the protein to be higher than 20, or so. The actual value of this important parameter is

Table 5
Same as in Table 4, only for PBE0 density functional

Redox state	ΔE_{elec}	$\Delta\Delta E_{elec}$	ΔG_{solv}	$\Delta\Delta G_{solv}$	$\Delta\Delta G_{shift}$	ΔpK_a	pK_a
In aqueous phase							
4-methylimidazole	+231.37	0	+53.49	0	0	0	6.6
Fe=O $Cu_B^{2+}(H_2O)$ oxidized	+216.11	−15.26	+70.67	+17.18	+1.92	+1.40	8.00
Fe=O $Cu_B^{+}(H_2O)$ reduced	+290.74	+59.37	+6.96	−46.53	+12.84	+9.35	15.95
In continuum dielectric of ε=4 (no protein charges)							
Fe=O $Cu_B^{2+}(H_2O)$ oxidized	+216.11	−15.26	+55.50	+2.01	−13.25	−9.65	−3.05
Fe=O $Cu_B^{+}(H_2O)$ reduced	+290.74	+59.37	+10.92	−42.57	+16.80	+12.24	18.84
In inhomogeneous dielectric of protein, ε = 4 and 80 (no protein charges)							
Fe=O $Cu_B^{2+}(H_2O)$ oxidized	+216.11	−15.26	+60.32	+6.83	−8.43	−6.14	0.46
Fe=O $Cu_B^{+}(H_2O)$ reduced	+290.74	+59.37	+12.75	−40.74	+18.63	+13.57	20.17
In continuum ε=4 (including protein charges)							
OORO	+216.11	−15.26	+85.81	+32.32	+17.06	+12.43	19.03
OORR	+290.74	+59.37	+43.00	−10.49	+48.88	+35.61	42.21
In protein (including dielectric inhomogeneity and protein charges)							
OORO	+216.11	−15.26	+66.55	+13.06	−2.20	−1.60	5.00
OORR	+290.74	+59.37	+20.96	−32.53	+26.84	+19.55	26.15
OORO (ε_{cavity}=20)	+216.11	−15.26	+70.55	+17.06	+1.80	+1.31	7.91
OORR (ε_{cavity}=20)	+290.74	+59.37	+25.66	−27.83	+31.54	+22.98	29.58

not known, however, a value higher than 20 does not seem to be unreasonable. (The work is underway in this group to determine the value of dielectric constant of water cavities in the direct simulation of water molecules in the enzyme cavities.)

The main conclusion of this part of calculations is that as in our previous work, where a much different (electronic and solvation) model of the Cu_B center was considered, here we find that the pK_a of His291 depends on the redox state of the Fe_{a3}–Cu_B center, so that in OORR state, it is certainly protonated, while in the OORO state it is most likely deprotonated. It means that when a chemical proton arrives to Fe_{a3}–Cu_B center, the state, according to our notation, changes from OORR to OORO, and the repulsion between the chemical proton and the proton on His291 is strong enough, so that the latter becomes deprotonated. This expulsion of the proton from His291 by the chemical proton is the key element of the pumping mechanism that we proposed.

The principal question that we were not able to address before, however, is about the chemical proton itself. Would it indeed go to the Fe_{a3}–Cu_B center at the expense of expelling the proton from His291? This question is discussed in the following sections.

3.3. The pK_a of H_2O/OH^- ligand to Cu_B

Considering two structures Fe═O $(HO^-)Cu^{2+}$ (HisH) and Fe═O $(H_2O)Cu^{2+}$ (HisH), we calculated the pK_a of H_2O ligand of the Cu_B center. MeIm compound was used as a reference. Table 6 lists the different contributions to the total solvation energy of the two compounds, together with the pK_a of H_2O ligand in the aqueous phase and in the protein–membrane–solvent system. Both B3LYP and PBE0 results are reported.

There are no experimental data for the pK_a of H_2O ligand in the binuclear complex in *CcO*. In fact, this is the key experimental uncertainty in the characterization of the enzyme. In aqueous solution (we stress that this is an artificial situation considered only for the sake of completeness), the calculated pK_a of 11.2 (B3LYP) to 11.9 (PBE0) for the ligated H_2O to Cu_B^{2+} metal center is close to our expectation. The pK_a of H_2O/OH^- couple in water is known to be 15.7. The ligation to Cu^{2+} metal center should definitely decrease the pK_a of H_2O ligand, however, not very significantly, considering that the H_2O (protonated) form is much better stabilized by a hydrogen-bond with the ferryloxy (Fe_{a3}=O) group than negatively charged OH^- group. Also, all formal charges are pretty well delocalized on both, histidine ligands and porphyrin ring, and additionally screened by high dielectric of aqueous phase, such that expected effect on the pK_a of water ligand is most likely to be very moderate in aqueous solution.

Within the protein, the computed pK_a of H_2O/OH^- ligand is found to be 8.5 to 9.6 in the state of the enzyme prior to pumping, i.e., when His291 is protonated. It means that there is a small driving force, which allows a chemical proton to enter the active site and form water molecule in the presence of Cu^{2+}, even when His291 is protonated. Given the uncertainties of calculations (see discussion of possible error bars below), the exact value of the driving force is difficult to compute accurately, and the conclusion should be taken cautiously.

Table 6
The pK_a value of water Cu_B ligand in the enzyme active site in Fe═O $Cu_B^{2+}(H_2O)$ (His291H) redox state of the binuclear complex

Compound	G_{Born}	G_q	G_{strain}	G_{solv}	Dielectric pK_a
B3LYP					
Fe═O $Cu_B^{2+}(HO^-)$(His291H)	−77.85	0.00	+8.32	−69.53	Water
Fe═O $Cu_B^{2+}(H_2O)$(His291H)	−147.20	0.00	+5.13	−142.07	
Δ(Depr.-Prot.)	+69.35	0.00	+3.19	+72.54	11.17 [a]
Fe═O $Cu_B^{2+}(HO^-)$(His291H)	−45.81	−16.07	+3.04	−58.84	Protein
Fe═O $Cu_B^{2+}(H_2O)$(His291H)	−109.43	−20.75	+2.50	−127.68	
Δ(Depr.-Prot.)	+63.62	+4.68	+0.54	+68.84	8.47 [a]
PBE0					
Fe═O $Cu_B^{2+}(HO^-)$(His291H)	−80.50	0.00	+8.77	−71.73	Water
Fe═O $Cu_B^{2+}(H_2O)$(His291H)	−145.31	0.00	+2.77	−142.54	
Δ(Depr. - Prot.)	+64.81	0.00	+6.00	+70.81	11.87 [b]
Fe═O $Cu_B^{2+}(HO^-)$(His291H)	−46.98	−16.19	+3.35	−59.82	Protein
Fe═O $Cu_B^{2+}(H_2O)$(His291H)	−109.69	−20.81	+2.55	−127.95	
Δ(Depr.-Prot.)	+62.71	+4.62	+0.80	+68.13	9.63 [b]

Solvation energies (in kcal/mol) are reported for the B3LYP and PBE0 density functional computations. The pK_as are calculated (see Eq. (6)) for the protein–membrane–solvent system ($\varepsilon_{prot}=\varepsilon_{memb}=4$, $\varepsilon_{sol}=80$) and for the binuclear complex solvated in a continuum aqueous phase ($\varepsilon_{sol}=80$). Methylimidazole is used as a model compound for the pK_a calculations.
Energy terms used in calculation of the pK_a of water Cu_B ligand in aqueous solution and within the protein:
[a] B3LYP

$$\Delta E_{elec}^{comp} = +222.66;\ \Delta E_{elec}^{MeIm} = +234.60;\ \Delta\Delta E_{elec} = -11.94;$$

$$\Delta G_{solv}^{comp,aq} = +72.54; \Delta G_{solv}^{MeIm,aq} = +54.83; \Delta\Delta G_{solv}^{aq} = +17.71;$$

$$\Delta G_{solv}^{comp,prot} = +68.84; \Delta\Delta G_{solv}^{prot} = +14.01; \Delta\Delta G_{vib} = +0.50.$$

[b] PBE0

$$\Delta E_{elec}^{comp} = +220.79; \Delta E_{elec}^{MeIm} = +231.37; \Delta\Delta E_{elec} = -10.58;$$

$$\Delta G_{solv}^{comp,aq} = +70.81; \Delta G_{solv}^{MeIm,aq} = +53.49; \Delta\Delta G_{solv}^{aq} = +17.32;$$

$$\Delta G_{solv}^{comp,prot} = +68.13; \Delta\Delta G_{solv}^{prot} = +14.64; \Delta\Delta G_{vib} = +0.50.$$

In fact, for the pump to work, the driving force for chemical proton when His291 is protonated is not necessary. What *is* necessary, however, is to have the driving force for the exchange of the chemical proton and the proton on His291. In other words, the question is will the chemical proton go to the OH^- group in the Fe_{a3}–Cu_B center, at the expense of expelling the proton from His291? This is a question about the energy of the pumping step. Not only this energy should be available, it should be large enough to push the proton through the electrochemical proton gradient of the membrane.

3.4. The free energy of the pumping step

As it was proposed earlier on the basis of pure continuum electrostatic calculations [11,12], the entrance of a chemical proton into the binuclear complex of *CcO* that converts OH^-

Table 7
The reaction free energy (ΔG_R) of the proton pumping step (in kcal/mol): Fe═O (HO^-)Cu^{2+} (HisH) ⇄ Fe═O (H_2O)Cu^{2+} (His^-) is calculated based on the B3LYP density functional electronic energies and the protein and reaction field solvation energy terms, see Eq. (8)

Dielectric medium [a] $\varepsilon_{prot}/\varepsilon_{cavity}$	ΔE_{elec} (1)	G_{1Born}	G_{2Born}	ΔG_{Born} (2)	G_{1q}	G_{2q}	ΔG_q (3)	ΔG_{solv} (2+3)	ΔG_R [b] (1+2+3)
Continuum 4	−2.26	−41.02	−42.81	−1.79	−38.29	−33.69	+4.60	+2.81	0.26
4/15	−2.26	−43.88	−46.80	−2.92	−22.44	−19.41	+3.03	+0.11	−2.44
4/20	−2.26	−44.30	−47.35	−3.05	−20.66	−17.93	+2.73	−0.32	−2.87
4/80	−2.26	−45.81	−49.04	−3.23	−16.07	−14.49	+1.58	−1.65	−4.20
10/20	−2.26	−52.73	−55.52	−2.79	−13.79	−13.00	+0.79	−2.00	−4.55
20/20	−2.26	−56.07	−58.69	−2.62	−10.96	−11.07	−0.11	−2.73	−5.28
Aqueous phase	−2.26	−69.49 [c]	−69.89 [c]	−0.40	0.00	0.00	0.00	−0.40	−3.16

[a] Calculations are done for the different dielectric conditions: in continuum dielectric of ε=4 (including protein charges); for the several cases where dielectric of protein (ε_{prot}) or the solvent filled cavities (ε_{cavity}) was varied; and for the QM system solvated in the aqueous phase without any external surrounding protein charges.
[b] The small contributions of the vibrational energy change (ΔG_{vib}=−0.50) and energy terms due to the strain ($G_{1strain}$=+3.04, $G_{2strain}$=+3.25 and ΔG_{strain}=+0.21, all in kcal/mol) are also taken into account, according to Eq. (8).
[c] Including corresponding strain energies in aqueous solution.

ligand to H_2O is a trigger for a proton pumping event which causes the deprotonation of His291 site and a release of a proton on the periplasmic (positive) side of the membrane.

The reaction free energy (ΔG_R) of a proton pumping step,

$$\underset{\text{initial state (1)}}{Fe=O(HO^-)Cu^{2+}(HisH)} \rightleftarrows \underset{\text{final state (2)}}{Fe=O(H_2O)Cu^{2+}(His^-)} \quad (7)$$

was calculated as follows:

$$\Delta G_R = G_{final(2)} - G_{initial(1)} = \Delta E_{elec} + \Delta G_{vib} + \Delta G_{Born} + \Delta G_q + \Delta G_{strain}, \quad (8)$$

where, ΔG_{vib} is the difference in the zero-point energy of two states, and other terms are the same as explained earlier in the text.

The values (in kcal/mol) of various energy terms used to calculate the reaction free energy of the proton pumping step are presented in Table 7 (B3LYP) and Table 8 (PBE0). The gas-phase DFT-B3LYP electronic energy (−2.26 kcal/mol), the difference in vibrational energy (−0.5 kcal/mol), and the Born-solvation energy due to the polarization (−3.23 kcal/mol) favor the exergonicity of the reaction, while the effect of the protein charges slightly disfavors the proton pumping step by +1.58 kcal/mol. The effect of the strain energy term is almost negligible. The total B3LYP reaction energy is −4.20 kcal/mol for the inhomogeneous dielectric of protein–membrane–solvent system where $\varepsilon_{prot}=\varepsilon_{memb}=4$ and $\varepsilon_{sol}=\varepsilon_{cavity}=80$. The calculation based on PBE0 density functional gives similar results with the corresponding terms: ΔE_{elec}=−4.68, ΔG_{vib}=−0.10, ΔG_{Born}=−3.54, ΔG_q=+1.61, ΔG_{strain}=+0.35 and total reaction free energy of −6.36 kcal/mol.

We also examine the dependence of the reaction energy on the various possible values for the dielectric constant of solvent within the water-filled cavities and epsilon of a protein region itself. A discussion of the appropriate values of these important parameters of the model system is beyond the scope of this paper and we are here only interested to explore the dependence of the main results and make qualitative conclusions. From the obtained results, one can see that a proton pumping step, as it is described in our proposed pumping mechanism [12], is energetically possible (and favorable) for a number of various dielectric models examined in this study. The DFT-PBE0 gives the reaction energies of a pumping step slightly higher than those of B3LYP, mainly due to the difference in electronic energy.

The calculations show that the examined pumping step is energetically feasible. The energy generated in this step is relatively small, yet enough to push a proton against the electrochemical gradient of the membrane. Indeed, the difference in the electrochemical potential across the mitochondrial membrane is about 200 meV (4.6 kcal/mol) and, assuming the high efficiency of *CcO*, one may expect the actual values of the pumping step energy around 5 kcal/mol, which is in an remarkably good agreement with our results. Given the

Table 8
The reaction free energy (ΔG_R) of the proton pumping step (in kcal/mol) is calculated based on Eq. (8), from the PBE0 density functional electronic and vibrational energies and the protein and reaction field solvation energy terms

Dielectric medium $\varepsilon_{prot}/\varepsilon_{solv}$	ΔE_{elec} (1)	G_{1Born}	G_{2Born}	ΔG_{Born} (2)	G_{1q}	G_{2q}	ΔG_q (3)	ΔG_{solv} (2+3)	ΔG_R [a] (1+2+3)
Continuum 4	−4.68	−42.14	−44.12	−1.98	−38.43	−33.72	+4.71	+2.73	−1.70
4/15	−4.68	−45.03	−48.22	−3.19	−22.57	−19.47	+3.10	−0.09	−4.52
4/20	−4.68	−45.46	−48.78	−3.32	−20.79	−18.00	+2.79	−0.53	−4.96
4/80	−4.68	−46.98	−50.52	−3.54	−16.19	−14.58	+1.61	−1.93	−6.36
10/20	−4.68	−54.22	−57.24	−3.02	−13.84	−13.03	+0.81	−2.21	−6.64
20/20	−4.68	−57.70	−60.53	−2.83	−10.97	−11.09	−0.12	−2.95	−7.38
Aqueous phase	−4.68	−71.73 [b]	−72.57 [b]	−0.84	0.00	0.00	0.00	−0.84	−5.52

[a] The small contributions of the vibrational energy change (ΔG_{vib}=−0.10) and energy terms due to the strain ($G_{1strain}$=+3.35, $G_{2strain}$=+3.70 and ΔG_{strain}=+0.35 all in kcal/mol) are also taken into account, according to Eq. (8).
[b] Including corresponding strain energies in aqueous solution.

uncertainties of the calculations, however, this most likely is a fortuitous agreement with the expectation. Most important and more reliable conclusion perhaps is that the free energy of the proposed pumping step is clearly not of a large and positive value, a result that would make the proposed scheme very unlikely. As it stands now, however, we conclude that the present calculations indeed support the proposal that the chemical proton expels the proton from His291, and triggers the pumping event.

4. Conclusion

In our earlier work, we evaluated the redox-dependent pK_as of Glu242 and His291 sites, although for His291 we used a rather different quantum-chemical model, which consisted of Cu_B complex alone [13]. Now, we repeated calculation using much different (and larger) model of the binuclear Fe_{a3}–Cu_B center. The results support our previous finding. This is quite remarkable because the models used in two calculations are rather different (they have quite different individual electronic and solvation energies, yet very similar total free energy of protonation). More importantly, with this new model of the binuclear center, we have managed to evaluate the free energy of the proposed pumping step.

The energetics of a proton pumping step during the F to F_p transtion (see Fig. 2B) is summarized in Fig. 5. For comparison, in Fig. 5A, results are shown for the model of Fe_{a3}–Cu_B complex in aqueous solution, and in Fig. 5B, inside of the protein. The energies of three protonation states of the binuclear complex are considered. In the initial state, His291 site is protonated and OH^- ligand is coordinated to Cu^{2+} center. This is a state before the entrance of the chemical proton into the active site. In the intermediate state, both His291 and OH^- are protonated, and in the final state, OH^- is protonated (i.e. H_2O), while His291 is deprotonated, with its proton ejected from the system.

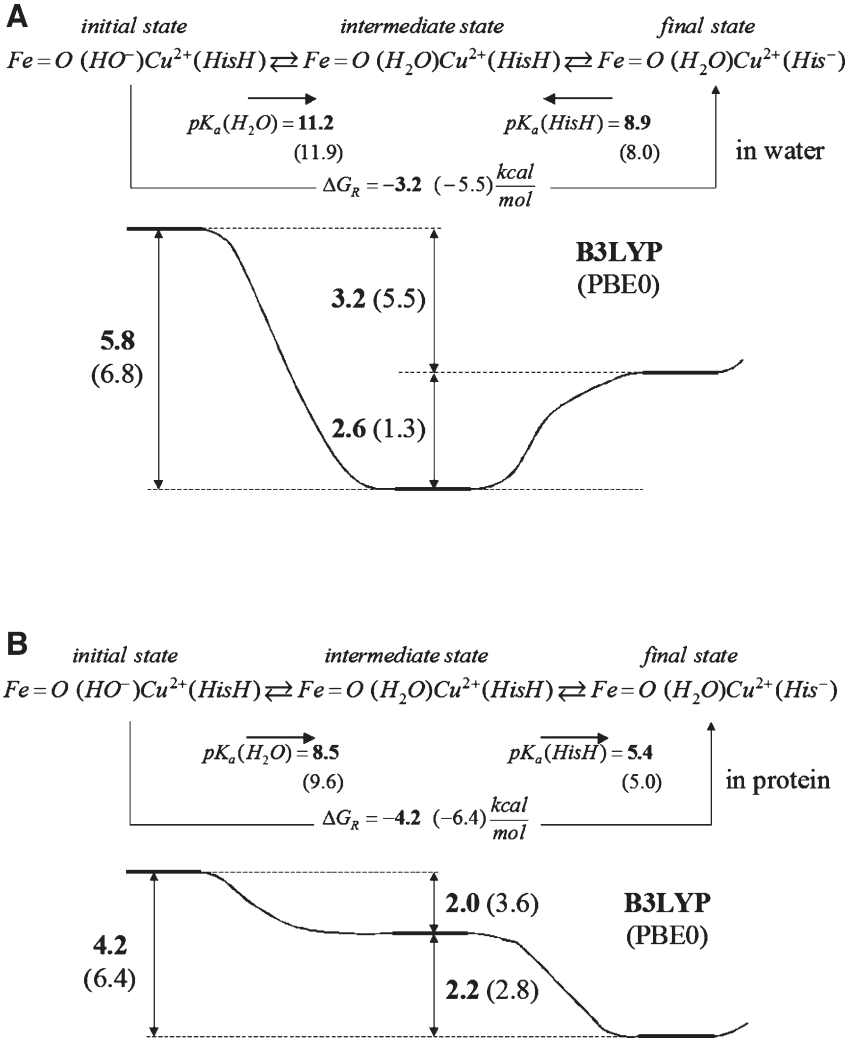

Fig. 5. Energy diagram of a proton pumping step obtained from the combined B3LYP (or PBE0) density functional/electrostatic solvation calculations, based on Eqs. (6) and (8), for the Fe_{a3}–Cu_B complex: (A) in aqueous solution and, (B) within the cytochrome *c* oxidase for the protein–membrane–solvent model system. The calculated pK_as of H_2O and His291 ligands of Cu_B^{2+} center are given along with the arrows showing a direction in which the reaction equilibrium is shifted. The reaction free energies (in kcal/mol) at pH = 7, shown in bold refer to B3LYP calculations, while PBE0 energies are reported in parentheses in normal font letters.

As shown in the figure, in the aqueous phase the most stable state is the intermediate one, with both OH^- *and* His291 protonated. The pumping is not achieved in this case. However, within the protein the [Fe═O $(H_2O)Cu^{2+}$ (His^-)] state becomes energetically most favorable one, therefore the entrance of the chemical proton to the binuclear center results in the pumping event. The change in the order of energy levels between aqueous solution and the protein is basically due to a large destabilization of the intermediate +2 state (the other two states have a charge of +1) in the low-epsilon dielectric of the protein. Accordingly, the main difference between the two cases obviously is in the increased proton–proton repulsion in the low dielectric of the protein medium, which results in the expulsion of the His291 proton by the chemical proton.

The energy generated in the pumping step was found to be between 4 and 6.5 kcal/mol at pH 7. This energy is sufficient to push a proton across the membrane potential gradient of about 200 mV. The estimated error bar in this type of calculations, however, is at least ±2 to 3 kcal/mol, and the prediction should be considered only as an indication of the likelihood of the proposed pumping scheme.

In summary, our present calculation point to feasibility of the pumping scheme in *CcO* shown in Fig. 2A. According to this scheme, upon an electron transfer to the binuclear center, the translocation of two protons, of which both originate on the negative side of the membrane, takes place. The first, "fast" proton protonates His291, while the second "slow" chemical proton arrives later to the binuclear center where it converts the OH^- to water. Due to the repulsion between the two protons, the first one is expelled to the positive side of the membrane. The kinetic treatment of the proposed model yields results that are in agreement with available measurements of the membrane potential generated by the enzyme [70]. Yet, a direct experimental test of the predicted redox dependency of His291 ligand would be desirable.

Acknowledgements

We would like to thank Dmitry Makhov for his helpful input. This work has been supported by the NSF grant and a research grant from the NIH (GM54052).

References

[1] M. Wikström, Proton translocation by bacteriorhodopsin and heme-copper oxidases, Curr. Opin. Struct. Biol. 8 (1998) 480–488.
[2] R.B. Gennis, How does cytochrome oxidase pump protons? Proc. Natl. Acad. Sci. U. S. A. 95 (1998) 12747–12749.
[3] H. Michel, J. Behr, A. Harrenga, A. Kannt, Cytochrome c oxidase: structure and spectroscopy, Annu. Rev. Biopys. Biomol. Struct. 27 (1998) 329–356.
[4] G.T. Babcock, M. Wikström, Oxygen activation and the conservation of energy in cell respiration, Nature 356 (1992) 301–309.
[5] S. Ferguson-Miller, G.T. Babcock, Heme-copper oxidase, Chem. Rev. 7 (1996) 2889–2907.
[6] . M. Wikström, A. Jasaitis, C. Backgren, A. Puustinen, M.I. Verkhovsky, The role of the D- and K-pathways of proton transfer in the function of the heam-copper oxidases, Biochim. Biophys. Acta 1459 (2000) 514–520.
[7] D. Zaslavsky, R.B. Gennis, Proton pumping by cytochrome oxidase: progress, problems and postulates, Biochim. Biophys. Acta 1458 (2000) 164–179.
[8] H. Michel, Cytochrome c oxidase: catalytic cycle and mechanism of proton pumping—A discussion, Biochemistry 38 (1999) 15129–15140.
[9] M. Wikström, Proton translocation by cytochrome c oxidase: a rejoinder to recent criticism, Biochemistry 39 (2000) 3515–3519.
[10] S. Han, S. Takahashi, D.L. Rousseau, Time dependence of the catalytic intermediates in cytochrome c oxidase, J. Biol. Chem. 275 (2000) 1910–1919.
[11] D.M. Popovic, A.A. Stuchebrukhov, Electrostatic study of proton pumping mechanism of bovine heart cytochrome *c* oxidase, J. Am. Chem. Soc. 126 (2004) 1858–1871.
[12] D.M. Popovic, A.A. Stuchebrukhov, Proton pumping mechanism and catalytic cycle of cytochrome *c* oxidase: Coulomb pump model with kinetic gating, FEBS Lett. 566 (2004) 126–130.
[13] D.M. Popovic, J. Quenneville, A.A. Stuchebrukhov, DFT/electrostatic calculations of pK_a values in cytochrome c oxidase, J. Phys. Chem., B 109 (2005) 3616–3626.
[14] X. Zheng, D.M. Medvedev, J. Swanson, A.A. Stuchebrukhov, Computer simulations of internal water in cytochrome *c* oxidase, Biochim. Biophys. Acta 1557 (2003) 99–106.
[15] M. Tashiro, A.A. Stuchebrukhov, Thermodynamic properties of internal water molecules in the hydrophobic cavity around the catalytic center of cytochrome *c* oxidase, J. Phys. Chem., B 109 (2005) 1015–1022.
[16] M.L. Verkhovskaya, A. Garcia-Horsman, A. Puustinen, J.-L. Rigaud, J.E. Morgan, M.I. Verkhovsky, M. Wikström, Glutamic acid 286 in subunit I of cytochrome bo3 is involved in proton translocation, Proc. Natl. Acad. Sci. U. S. A. 94 (1997) 10128–10131.
[17] P. Adelroth, M.S. Ek, D.M. Mitchell, R.B. Gennis, P. Brzezinski, Glutamate 286 in cytochrome aa3 from *Rhodobacter sphaeroides* is involved in proton uptake during the reaction of the fully-reduced enzyme with dioxygen, Biochemistry 36 (1997) 13824–13829.
[18] M. Wikstrom, A. Jasaitis, C. Backgren, A. Puustinen, M.I. Verkhovsky, The role of the D- and K-pathways of proton transfer in the function of the haem-copper oxidases, Biochim. Biophys. Acta 1459 (2000) 514–520.
[19] D. Zaslavsky, R.B. Gennis, Proton pumping by cytochrome oxidase: progress, problems and postulates, Biochim. Biophys. Acta 1458 (2000) 164–179.
[20] D.M. Popovic, A.A. Stuchebrukhov, Proton exit channels in cytochrome c oxidase, J. Phys. Chem., B 109 (2005) 1999–2006.
[21] J.M. Mouesca, J.L. Chen, L. Noodleman, D. Bashford, D.A. Case, Density functional/Poisson–Boltzmann calculations of redox potentials for iron–sulfur clusters, J. Am. Chem. Soc. 116 (1994) 11898–11914.
[22] J. Li, C.L. Fischer, J.L. Chen, D. Bashford, L. Noodleman, Calculation of redox potentials and pK_a values of hydrated transition metal cations by a combined density functional and continuum dielectric theory, J. Phys. Chem. 96 (1996) 2855–2866.
[23] J. Li, M.R. Nelson, C.Y. Peng, D. Bashford, L. Noodleman, Incorporating protein environments in density functional theory: a self-consistent reaction field calculation of redox potentials of [2Fe2S] clusters in ferredoxin and phthalate dioxygenase reductase, J. Phys. Chem., A 102 (1998) 6311–6324.
[24] J. Li, C.L. Fisher, R. Konecny, D. Bashford, L. Noodleman, Density functional and electrostatic calculations of manganese superoxide dismutase active site complexes in protein environments, Inorg. Chem. 38 (1999) 929–939.
[25] G.M. Ullmann, L. Noodleman, D.A. Case, Density functional calculation of pK_a values and redox potentials in the bovine Rieske iron–sulfur protein, J. Biol. Inorg. Chem. 7 (2002) 632–639.
[26] J.L. Chen, L. Noodleman, D.A. Case, D. Bashford, Incorporating solvation effects into density functional electronic structure calculations, J. Phys. Chem. 98 (1994) 11059–11068.
[27] B. Kallies, R. Mitzner, pK_a values of amines in water from quantum mechanical calculations using a polarized dielectric continuum representation of the solvent, J. Phys. Chem., B 101 (1997) 2959–2967.
[28] W.H. Richardson, C. Peng, D. Bashford, L. Noodleman, D.A. Case,

Incorporating solvation effects into density functional theory: calculation of absolute acidities, Int. J. Quant. Chem. 61 (1997) 207–217.
[29] J. Quenneville, D.M. Popovic, A.A. Stuchebrukhov, Redox-dependent pK_a of CuB histidine ligand in cytochrome c oxidase, J. Phys. Chem., B 108 (2004) 18383–18389.
[30] S. Yoshikawa, K. Shinzawa-Itoh, R. Nakashima, R. Yaono, E. Yamashita, N. Inoue, M. Yao, M.J. Fei, C.P. Libeu, T. Mizushima, H. Yamaguchi, T. Tomizaki, T. Tsukihara, Redox-coupled structural changes in bovine heart cytochrome c oxidase, Science 280 (1998) 1723–1729.
[31] P. Hohenberg, W. Kohn, Inhomogeneous electron gas, Phys. Rev. 136 (1964) B864–B871.
[32] K. Kohn, L.J. Sham, Self-consistent equations including exchange and correlation effects, Phys. Rev. 140 (1965) A1133–A1136.
[33] Jaguar 5.5, S., L.L.C., Portland, OR, 1991–2003. ed.
[34] A.D. Becke, Density-functional thermochemistry. III. The role of exact exchange, J. Chem. Phys. 98 (1993) 5648.
[35] J.P. Perdew, M. Ernzerhof, K. Burke, Rationale for mixing exact exchange with density functional approximations, J. Chem. Phys. (1996) 9982–9990.
[36] M.R.A. Blomberg, P.E.M. Siegbahn, G.T. Babcock, M. Wikström, Modeling cytochrome oxidase: a quantum chemical study of the O–O bond cleavage mechanism, J. Am. Chem. Soc. 122 (2000) 12848–12858.
[37] M.R.A. Blomberg, P.E.M. Siegbahn, G.T. Babcock, M. Wikström, O–O bond splitting mechanism in cytochrome oxidase, J. Inorg. Biochem. 80 (2000) 261–269.
[38] P.E.M. Siegbahn, M.R.A. Blomberg, M.L. Blomberg, Theoretical study of the energetics of proton pumping and oxygen reduction in cytochrome oxidase, J. Phys. Chem., B 107 (2003) 10946–10955.
[39] C. Adamo, V. Barone, Toward reliable density functional methods without adjustable parameters: the PBE0 model, J. Chem. Phys. 110 (1999) 6158–6170.
[40] V.N. Staroverov, G.E. Scuseria, J. Tao, J.P. Perdew, Comparative assessment of a new nonempirical density functional: molecules and hydrogen-bonded complexes, J. Chem. Phys. 119 (2003) 12129–12137.
[41] P.J. Hay, W.R. Wadt, Ab initio effective core potentials for molecular calculations. Potentials for K to Au including the outermost core orbitals, J. Chem. Phys. 82 (1985) 299–310.
[42] T. Clark, J. Chandrasekhar, G.W. Spitznagel, P.v.R. Schleyer, Efficient diffuse function-augmented basis sets for anion calculations. III. The 3–21 +G basis set for first-row elements, Li–F, J. Comput. Chem. 4 (1983) 294–301.
[43] M.J. Frisch, J.A. Pople, J.S. Binkley, Self-consistent molecular orbital methods 25. Supplementary functions for Gaussian basis sets, J. Chem. Phys. 80 (1984) 3265–3269.
[44] R. Krishnan, J.S. Binkley, R. Seeger, J.A. Pople, Self-consistent molecular orbital methods. XX. A basis set for correlated wave functions, J. Chem. Phys. 72 (1980) 650–654.
[45] A.D. McLean, S.G. Chandler, Contracted Gaussian basis sets for molecular calculations. I. Second row atoms, Z=11–18, J. Chem. Phys. 72 (1980) 5639–5648.
[46] R. Ditchfield, W.J. Hehre, J.A. Pople, Self-consistent molecular-orbital methods. IX. An extended Gaussian-type basis for molecular-orbital studies of organic molecules, J. Chem. Phys. 54 (1971) 724–728.
[47] W.J. Hehre, R. Ditchfield, J.A. Pople, Self-consistent molecular orbital methods. XII. Further extensions of Gaussian-type basis sets for use in molecular orbital studies of organic molecules, J. Chem. Phys. 56 (1972) 2257–2261.
[48] W.J. Hehre, J.A. Pople, Self-consistent molecular orbital methods. XIII. An extended Gaussian-type basis for boron, J. Chem. Phys. 56 (1972) 4233–4234.
[49] J.S. Binkley, J.A. Pople, Self-consistent molecular orbital methods. XIX. Split-valence Gaussian-type basis sets for beryllium, J. Chem. Phys. 66 (1977) 879–880.
[50] P.C. Hariharan, J.A. Pople, The influence of polarization functions on molecular orbital hydrogenation energies, Theor. Chim. Acta 28 (1973) 213–222.
[51] M.M. Francl, W.J. Pietro, W.J. Hehre, J.S. Binkley, M.S. Gordon, D.J. DeFrees, J.A. Pople, Self-consistent molecular orbital methods. XXIII. A polarization-type basis set for second-row elements, J. Chem. Phys. 77 (1982) 3654–3665.
[52] M.T. Green, Imidazole ligated compound I intermediates: the effects of hydrogen bonding, J. Am. Chem. Soc. 122 (2000) 9495–9499.
[53] M.T. Green, The structure and spin coupling of catalase compound I: a study of non-covalent effects, J. Am. Chem. Soc. 123 (2001) 9218–9219.
[54] D.J. Tannor, B. Marten, R. Marphy, R.A. Friesner, D. Sitkoff, A. Nicholls, M. Ringnalda, W.A. Goddard III, B. Honig, Accurate first principles calculation of molecular charge distributions and solvation energies from ab initio quantum mechanics and continuum dielectric theory, J. Am. Chem. Soc. 116 (1994) 11875–11882.
[55] B. Marten, K. Kim, C. Cortis, R.A. Friesner, R.B. Murphy, M.N. Ringnalda, D. Sitkoff, B. Honig, New model for calculation of solvation free energies: correction of self-consistent reaction field continuum dielectric theory for short-range hydrogen-bonding effects, J. Phys. Chem. 100 (1996) 11775–11788.
[56] C.M. Breneman, K.B. Wiberg, Determining atom-centered monopoles from molecular electrostatic potentials. The need for high sampling density in formamide conformational analysis, J. Comput. Chem. 11 (1990) 361–373.
[57] D. Bashford, K. Gerwert, Electrostatic calculations of the pK_a values of ionizable groups in bacteriorhodopsin, J. Mol. Biol. 224 (1992) 473–486.
[58] D. Bashford, An object-oriented programming suite for electrostatic effects in biological molecules, in: Y. Ishikawa, R.R. Oldehoeft, J.V.W. Reynders, M. Tholburn (Eds.), Scientific Computing in Object-Oriented Parallel Environments, Springer, Berlin, 1997, pp. 233–240.
[59] K. Sharp, B. Honig, Electrostatic interactions in macromolecules: theory and applications, Annu. Rev. Biophys. Biophys. Chem. 19 (1990) 301–332.
[60] T. Simonson, D. Perahia, Internal and interfacial dielectric properties of cytochrome *c* from molecular dynamics in aqueous solution, Proc. Natl. Acad. Sci. U. S. A. 92 (1995) 1082–1086.
[61] T. Simonson, C.L. Brooks, Charge separation and the dielectric constant of proteins: insights from molecular dynamics, J. Am. Chem. Soc. 118 (1996) 8452–8458.
[62] A. Warshel, A. Papazyan, Electrostatic effects in macromolecules: fundamental concepts and practical modeling, Curr. Opin. Struct. Biol. 8 (1998) 211–217.
[63] A.D. MacKerell Jr., D. Bashford, M. Bellot, R.L. Dunbrack Jr., J.D. Evanseck, M.J. Field, S. Fischer, J. Gao, H. Guo, S. Ha, D. Joseph-McCarthy, L. Kuchnir, K. Kuczera, F.T.K. Lau, C. Mattos, S. Michnick, T. Ngo, D.T. Nguyen, B. Prodholm, I. Reiher, W. E., B. Roux, M. Schlenkrich, J.C. Smith, R. Stote, J. Straub, M. Watanabe, J. Wiórkiewicz-Kuczera, D. Yin, M. Karplus, All-atom empirical potential for molecular modeling and dynamics studies of proteins, J. Phys. Chem. 102 (1998) 3586–3616.
[64] D.M. Popovic, S.D. Zaric, B. Rabenstein, E.W. Knapp, Artificial cytochrome b: computer modeling and evaluation of redox potentials, J. Am. Chem. Soc. 123 (2001) 6040–6053.
[65] D.M. Popovic, A. Zmiric, S.D. Zaric, E.W. Knapp, Energetics of radical transfer in DNA photolyase, J. Am. Chem. Soc. 124 (2002) 3775–3782.
[66] P. Vagedes, B. Rabenstein, J. Åqvist, J. Marelius, E.W. Knapp, The deacylation step of acetylholinesterase: computer simulation studies, J. Am. Chem. Soc. 122 (2000) 12254–12262.
[67] B. Rabenstein, E.W. Knapp, Calculated pH-dependent population of CO-myoglobin coformers, Biophys. J. 80 (2001) 1141–1150.
[68] M. Tanokura, ^{1}H-NMR study on the tautomerism of the imidazole ring of histidine residues: I. Microscopic pK values and molar ratios of tautomers in histidine-containing peptides, Biochem. Biophys. Acta 742 (1983) 576–585.
[69] C. Tanford, R. Roxby, Interpretation of protein titration curves. Application to lysozyme, Biochemistry 11 (1972) 2192–2198.
[70] D.M. Medvedev, E.S. Medvedev, A.I. Kotelnikov, A.A. Stuchebrukhov, Analysis of the kinetics of the membrane potential generated by cytochrome *c* oxidase upon single electron injection, Biochem. Biophys. Acta 1710 (2005) 47–56.